

Robust load frequency control for networked power system with renewable energy via fractional-order global sliding mode control

Xinxin Lv^{1,2}  | Yonghui Sun¹ | Wenqiang Hu³  | Venkata Dinavahi² 

¹ College of Energy and Electrical Engineering, Hohai University, Nanjing 210098, China

² Department of Electrical and Computer Engineering, University of Alberta, Edmonton T6G 2V4, Canada

³ School of Electrical Engineering, Southeast University, Nanjing 210096, China

Correspondence

Yonghui Sun, College of Energy and Electrical Engineering, Hohai University, Nanjing 210098, China. sunyhui168@gmail.com

Funding information

National Natural Science Foundation of China, Grant/Award Number: 62073121; Natural Sciences and Engineering Research Council of Canada, Grant/Award Number: NSERC; Six Talent Peaks High Level Project of Jiangsu Province, Grant/Award Number: 2017-XNY004; Innovation Team of Six Talent Peaks Project of Jiangsu Province, Grant/Award Number: 2019-TD-XNY-001; China Scholarship Council, Grant/Award Number: CSC

Abstract

Owing to random load changes and transmission time delays in interconnected power systems with renewable energy, the load frequency control scheme has become one of the main methods to keep stability and security of power systems. To relieve communication burden and increase network utilisation, an adaptive event-triggered scheme is explored. Then, a new fractional-order global sliding mode control scheme comprising the fractional-order term in the sliding surface is adopted to improve robustness of load frequency control. The fractional-order term generates a new degree of freedom and more adjustable parameters to improve control performance. Furthermore, the Markov theory is applied in the modelling process to better describe the uncertainty of parameters and external disturbances. The stability and stabilisation criteria for multi-area power systems load frequency control are put forward by employing the improved Lyapunov function and integral inequalities with auxiliary functions. Finally, two simulation examples containing a two-area power system and modified IEEE 39-bus New England test power system with three wind farms are presented to investigate the effectiveness of the proposed method.

1 | INTRODUCTION

Load frequency control (LFC) is one of the significant measures to maintain safety and stability of power systems [1]. When power systems suffer from disturbances, LFC can be applied to keeping frequency deviations to zero, and maintaining exchange power of interconnected power systems to reference values [2, 3]. With the enhancement of environmental standards, the share of renewable energy and energy storage units has increased dramatically, which reduces energy consumption and improves energy utilisation efficiency [4, 5]. The application of turbine technologies makes it possible for wind farms to participate in the power system with a consolidated performance. However, owing to power resource instability of the wind power generation, the demands for operating reserve have increased [6]. To tackle this, the energy storage units are proposed in power system to balance instantaneous mismatch between generation and

demand. Inevitably, the introduction of wind power generation and energy storage units greatly increase difficulty and complexity of power systems LFC [7, 8].

Meanwhile, the open communication infrastructure is widely used in power systems to implement signal transmission and information communication where the control areas are interlinked through tie-lines, which has received increasing research attentions with their advantages of low cost and flexibility [9–11]. However, the severe competition of many loads and generation units for the limited network utilisation will appear if abundant data accesses to the network simultaneously [12,13]. Accordingly, event-triggered scheme is performed on the networked power system for reducing energy consumption and the transmission frequency of redundant information [14, 15]. More specifically, only when predetermined trigger condition is fulfilled, sampled information can be transmitted to controller [16]. Although the threshold cannot be adaptively

This is an open access article under the terms of the [Creative Commons Attribution](https://creativecommons.org/licenses/by/4.0/) License, which permits use, distribution and reproduction in any medium, provided the original work is properly cited.

© 2021 The Authors. *IET Renewable Power Generation* published by John Wiley & Sons Ltd on behalf of The Institution of Engineering and Technology

adjusted based on the dynamics of the networked power system, superfluous sampled information is transmitted over the networks. Therefore, it is highly necessary and meaningful to adopt the adaptive event-triggered (AET) scheme with adaptively adjusted threshold into networked power system LFC.

Considering the grid performance standards, massive control strategies, for example, optimal fuzzy-based PID droop control, active disturbance rejection control and generalised active disturbance rejection control, are developed in power system LFC [2, 17, 18]. The sliding mode control (SMC) is widely employed in power system LFC due to its robustness in parameters variation and external disturbances [19–21]. Some improved SMC schemes, for example, full order SMC [22], SMC with adaptive learning strategy [23], and the passivity-design of SMC [24] are utilised in power system LFC to improve the control performance. However, better robustness is still expected when power systems encounter heavily oscillations. Very recently, the fractional calculus has been proposed extending integer differentiation and integration into fractional orders [25, 26]. It is widely employed in modelling and control applications which can accurately characterise dynamics and behaviours of real systems [27–29]. Thus, the effectiveness of the fractional-order term adopted in improved SMC scheme need to be investigated in detail.

Motivated by the challenges of renewable energy and load disturbances, open communication infrastructures, and parameter uncertainties in networked power systems, the robust LFC based on AET scheme and fractional-order global sliding mode control (FOGSMC) is proposed in this paper. The wind power and energy storage systems are considered in this networked power system. Meanwhile, the proposed AET scheme significantly reduces transmission of the redundant information while preserving the control scheme's performance. Owing to transmission time delay, external disturbances and uncertain renewable energies in power system, the robust LFC for networked power system with renewable energy is studied in this paper. The novel FOGSMC which has outstanding robust performance is first employed in the networked power system LFC scheme to resist load disturbances and system parameter uncertainties. The proposed control scheme is placed on the second layer, and robustness can be enforced on tertiary level as well [30–33]. Additionally, Markov theory is employed to build the multi-area LFC model dealing with unknown modelling errors in the modelling process. By utilising improved Lyapunov stability theory and integral inequality with auxiliary function, the stability and stabilisation criteria are provided. Therefore, the following improvements are proposed:

i. Considering the rapid load changes and model parameter uncertainties, the FOGSMC is proposed in this paper for improving robustness of the power system LFC. On the one hand, the GSMC has robust stability during the entire control process while keeping the basic performance of traditional SMC. On the other hand, the fractional term is adopted in the FOGSMC to provide new degrees of freedom. Compared with integer order control, the FOGSMC with fractional term generates more adjustable parameters and improves control performance.

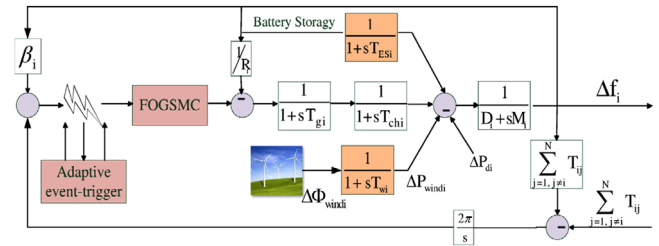


FIGURE 1 Transfer function model of multi-area time-delay hybrid power system

ii. An AET scheme is presented to mitigate transmission burden in multi-area power systems while maintaining FOGSMC performance and system dynamic properties. In the proposed AET scheme, the threshold can be adaptively adjusted by present and last moment signals, which can sharply reduce the number of transmitted data and greatly enhance network communication utilisation [34, 35].

iii. In the Lyapunov stability theory, constructing the improved Lyapunov function and estimating its derivatives are key elements to reduce the conservatism [10], in which triple integrals are adopted in the improved Lyapunov function to reduce the conservatism of the derived linear matrix inequality (LMI), and integral inequalities with auxiliary functions are introduced in estimating derivatives of the Lyapunov function to produce tighter bounds of transmission time delay than [32, 33].

The remainder of this paper is organised as follows. In Section 2, the Markov theory is introduced to build the delay-dependent multi-area power system LFC model comprising FOGSMC and AET scheme. Section 3 analyses the stability and stabilisation of the multi-area power system based on LMI. Simulation results and comparative analysis are shown in Section 4. Section 5 presents the conclusion of this work.

2 | PROBLEM STATEMENT

Even though the real power system is a complex non-linear dynamic system, the linearised model can be used to describe the system as the load deviation is very small when the system operates at the nominal point. The block diagram of the studied multi-area LFC considering wind power and energy storage is presented in Figure 1, where the AET scheme and FOGSMC are applied. The parameters of the i th control area are listed in Table 1.

2.1 | LFC model with transmission time delays

Dynamic model of the studied multi-area power system can be described as follows:

$$\begin{cases} \dot{x}(t) = Ax(t) + Bu(t) + F\omega(t) \\ y(t) = Cx(t), \end{cases} \quad (1)$$

TABLE 1 Notations

Symbol	Quantity
ΔP_{di}	Load deviation
ΔP_{mi}	Generator mechanical output deviation
ΔP_{vi}	Valve position deviation
ΔP_{tie-i}	Tie-line active power deviation
ΔP_{windi}	Output power fluctuation of the wind turbine generator
ΔP_{Bi}	Output power fluctuation of the battery
Δf_i	Frequency deviation
$\Delta \Phi_{windi}$	Wind power deviation
M_i	Moment of inertia
D_i	Generator damping coefficient
T_{gi}	Time constant of the governor
T_{chi}	Time constant of the turbine
T_{wi}	Time constant of the wind turbine
T_{ESi}	Time constant of the battery
R_i	Speed drop
β_i	Frequency bias factor
T_{ij}	Tie-line synchronising coefficient
ACE_i	Area control error

where

$$x_i(t) = [\Delta f_i \Delta P_{mi} \Delta P_{vi} \Delta P_{windi} \Delta P_{Bi} \int ACE_i \Delta P_{tie-i}]^T$$

$$x(t) = [x_1^T(t) x_2^T(t) x_3^T(t) \dots x_n^T(t)]^T$$

$$u(t) = [u_1^T(t) u_2^T(t) u_3^T(t) \dots u_n^T(t)]^T$$

$$\omega_i(t) = [\Delta P_{di} \Delta \Phi_{windi}]^T, A_{ij} = [(7, 1) = -2\pi T_{ij}]$$

$$y_i(t) = [ACE_i \int ACE_i]^T, B = \text{diag}\{B_1, \dots, B_n\}$$

$$\omega(t) = [\omega_1^T(t) \omega_2^T(t) \omega_3^T(t) \dots \omega_n^T(t)]^T$$

$$y(t) = [y_1^T(t) y_2^T(t) y_3^T(t) \dots y_n^T(t)]^T$$

$$A_{ii} = \begin{bmatrix} (1, 1) = \frac{-D}{M_i}, (1, 2) = \frac{1}{M_i}, (1, 4) = \frac{1}{M_i}, \\ (1, 5) = \frac{1}{M_i}, (1, 7) = \frac{-1}{M_i}, (2, 2) = \frac{-1}{T_{chi}}, \\ (2, 3) = \frac{1}{T_{chi}}, (3, 1) = \frac{-1}{RT_{gi}}, (3, 3) = \frac{-1}{T_{gi}}, \\ (4, 4) = \frac{-1}{T_{wi}}, (5, 1) = \frac{1}{T_{ESi}}, \\ (5, 5) = -\frac{1}{T_{ESi}}, (6, 1) = \beta_i, \\ (6, 6) = 1, (7, 1) = 2\pi \sum_{j=1, j \neq i}^n T_{ij} \end{bmatrix}$$

$$A = \begin{bmatrix} A_{11} & \dots & A_{1n} \\ \vdots & \ddots & \vdots \\ A_{n1} & \dots & A_{nn} \end{bmatrix}$$

$$B_i = \begin{bmatrix} 0 & 0 & \left(\frac{1}{T_{gi}}\right)^T & 0 & 0 & 0 & 0 \end{bmatrix}^T$$

$$C_i = \begin{bmatrix} \beta_i & 0 & 0 & 0 & 0 & 0 & 1 \\ 0 & 0 & 0 & 0 & 0 & 1 & 0 \end{bmatrix}$$

$$F_i = \begin{bmatrix} \frac{-1}{M_i^T} & 0 & 0 & 0 & 0 & 0 & 0 \\ 0 & 0 & 0 & \frac{1}{T_{wi}} & 0 & 0 & 0 \end{bmatrix}^T$$

$$C = \text{diag}\{C_1, \dots, C_n\}, F = \text{diag}\{F_1, \dots, F_n\}$$

The ACE signal for each control area can be expressed as

$$ACE_i = \beta_i \Delta f_i + \Delta P_{tie-i}. \quad (2)$$

2.2 | Fractional-order global sliding mode control scheme

Fractional calculus is a generalisation of the basic process of integral and differential into fractional order. To stabilise the power system with randomness and uncertainty, the new FOGSMC scheme incorporating a fractional-order term in the sliding surface is proposed in the following.

The fractional-order operator, shown as (3), contains the fractional derivative and the fractional integral in a single expression.

$${}_a D_t^{\alpha_1} = \begin{cases} \frac{d^{\alpha_1}}{dt^{\alpha_1}} & \alpha_1 > 0 \\ 1 & \alpha_1 = 0 \\ \int_a^t (ds)^{-\alpha_1} & \alpha_1 < 0 \end{cases} \quad (3)$$

where a and t are limits of the operator. For analytical simplification, ${}_a D_t^{\alpha_1}$ can be denoted as D^{α_1} .

The fractional-order global sliding surface is defined as

$$s(t) = Gx(t) - \int_0^t G(A - BKC)x(\tau) d\tau - f(t) + \mu D^{\alpha_1 - 1} x(t), \quad (4)$$

where $f(t)$ is a function designed specially to achieve global sliding mode, K means the controller gain to be designed, and μ

denotes the coefficient of fractional-order term. According to the definition of $f(t)$ in [36], it can be designed as following:

$$f(t) = f(0)e^{-lt}, \quad (5)$$

where $l > 0$.

The ideal sliding surface should satisfy: $s(t)=0$ and $\dot{s}(t) = 0$. Thus, the equivalent sliding mode control law is expressed as following:

$$\begin{aligned} u_{eq}(t) = & -KCx(t) - (GB)^{-1}GF\omega(t) + (GB)^{-1}\dot{f}(t) \\ & - \mu(GB)^{-1}D^{\alpha_1}x(t). \end{aligned} \quad (6)$$

Then the studied power system model can be revised as

$$\dot{x}(t) = Ax(t) - BKCx(t) + \tilde{F}\tilde{\omega}(t), \quad (7)$$

where

$$\begin{aligned} \tilde{\omega}(t) = & \left[\omega^T(t) \dot{f}^T(t) (D^{\alpha_1}x(t))^T \right]^T, \\ \tilde{F} = & [F - B(GB)^{-1}GF \quad 1 \quad \mu] \end{aligned}$$

Remark 1. In the designed sliding surface, the fractional-order term D^{α_1} and global function $f(t)$ are all considered. The fractional-order term generates a new degree of freedom to enhance control performance better than [20, 21, 36]. Besides, GSMC has fast response and robust performance, which can be applied to improve transient performance of the system. Therefore, the proposed FOGSMC scheme has satisfactory performance to stabilise the studied power system.

2.3 | Adaptive event-triggered scheme

Owing to transmission time delays in networked environment, the sampled data $ACE_i(t)$ is probably not be utilised at the certain time t . Then the controller input is described as

$$y(t) = Cx(t_k b), t \in [t_k b + d(t_k), t_{k+1} b + d(t_{k+1})], \quad (8)$$

where $t_k b$ means the transmitted instant of $x(t_k b)$ and b denotes the constant sampling period. Transmission delays caused by the network are considered as $d(t_k) \in [d_1, d_2]$, where $d_1 = \min(d(t_k))$, $d_2 = \max(d(t_k))$, $d_{12} = d_2 - d_1$, $\dot{d} = \dot{d}(t_k) = \lim_{\Delta t_k \rightarrow 0} \frac{d(t_k + \Delta t_k) - d(t_k)}{\Delta t_k}$.

In the event-triggered scheme, the sampled signal packets will be transmitted if the defined triggering condition is satisfied [34, 36]. However, the triggering threshold is predetermined in this scheme. There will still be a large of superfluous information transmitted to controller. In order to reduce

the transmission frequency of irrelevant information and save more network resources, the AEt scheme is employed to make triggering threshold adaptively adjustable. The AEt criterion is designed as

$$\begin{aligned} & [x(t_k b + jb) - x(t_k b)]^T \Phi_r [x(t_k b + jb) - x(t_k b)] \\ & > \lambda(t_k b) x(t_k b)^T \Phi_r x(t_k b), \end{aligned} \quad (9)$$

where Φ_r is an unknown positive matrix.

Comparing with the preset triggering threshold λ in [15], the $\lambda(t_k b)$ in (9) will be adaptively adjusted according to past and current transmitted packets:

$$\lambda(t_k b) = \max(\lambda_m, \eta \lambda(t_{k-1} b)), \quad (10)$$

where $\lambda_m > 0$ and

$$\eta = \begin{cases} 0, & \text{if } \|x(t_k b)\| \geq \|x(t_{k-1} b)\| \\ 1 - \frac{2\alpha_2}{\pi} \arctan \\ \left(\frac{\|x(t_k b)\| - \|x(t_{k-1} b)\|}{\|x(t_k b)\|} \right) & \text{otherwise} \end{cases}$$

2.4 | Markov model considering time delay

By considering transmission time delays, the studied multi-area LFC based on AEt and FOGSMC can be derived as

$$\dot{x}(t) = Ax(t) - BKCx(t) - BKCx(t - d(t)) + \tilde{F}\tilde{\omega}(t), \quad (11)$$

where

$$e(t) = \begin{cases} 0, & k \in \Omega_0 \\ x(t_k b) - x(t_k b + mb), & k \in \Omega_m \\ x(t_k b) - x(t_k b + jb), & k \in \Omega_j \end{cases}$$

and $j = \sup\{m \in N \mid t_k b + mb < t_{k+1} b, m = 1, 2, \dots\}$.

In the modelling procedure, there are many uncertain influences of transmission time delays and external disturbances. In real networks, the current transmission time delays are related with previous delays. Thus, the Markov chain is introduced into this paper to model the random transmission time delays [35]. The finite-state Markov process is described as

$$P[r_s(t + \Delta t) = j \mid r_s(t) = i] = p_{ij}, \quad (12)$$

$$0 \leq i, j \leq L, 0 \leq \pi_{ij} \leq 1, \sum_{j=0}^L \pi_{ij} = 1. \quad (13)$$

Thus, the multi-area LFC model can be expressed as the following Markov jump linear system model:

$$\dot{x}(t) = Ax(t) - BK_r C e(t) - BK_r C x(t - d(t)) + \tilde{F} \tilde{\omega}(t). \quad (14)$$

For analytical convenience, $K(r(t))$ is denoted as K_r .

Before presenting the main results, the following lemmas are introduced in advance.

Lemma 1 [36]: Let $Z_1 = Z_1^T$, $0 < Z_2 = Z_2^T$ and Z_3 be real matrices of appropriate dimensions, then $Z_1 + Z_3^T Z_2^{-1} Z_3 < 0$, if and only if $\begin{bmatrix} Z_1 & Z_3^T \\ Z_3 & -Z_2 \end{bmatrix} < 0$ or $\begin{bmatrix} -Z_2 & Z_3 \\ Z_3^T & Z_1 \end{bmatrix} < 0$.

Lemma 2 [37]: For a positive definite matrix $R > 0$, and a differentiable function $\{x(u)|u \in [a, b]\}$, the following inequalities hold:

$$\int_a^b \int_a^b \dot{x}^T(\alpha) \dot{x}(\alpha) d\alpha d\beta > 2\Omega_1^T R \Omega_1 + 4\Omega_2^T R \Omega_2$$

$$\int_a^b \int_a^a \dot{x}^T(\alpha) \dot{x}(\alpha) d\alpha d\beta > 2\Omega_3^T R \Omega_3 + 4\Omega_4^T R \Omega_4$$

where

$$\Omega_1 = x(b) - \frac{1}{b-a} \int_a^b x(\alpha) d\alpha,$$

$$\Omega_2 = x(b) + \frac{2}{b-a} \int_a^b x(\alpha) d\alpha - \frac{6}{(b-a)^2} \int_a^b \int_a^b x(\alpha) d\alpha d\beta,$$

$$\Omega_3 = x(a) - \frac{1}{b-a} \int_a^b x(\alpha) d\alpha,$$

$$\Omega_4 = x(a) - \frac{4}{b-a} \int_a^b x(\alpha) d\alpha + \frac{6}{(b-a)^2} \int_a^b \int_a^b x(\alpha) d\alpha d\beta.$$

3 | STABILITY AND STABILISATION ANALYSIS OF MULTI-AREA LFC

In this section, improved Lyapunov function and integral inequality with auxiliary function are employed to build the stability and stabilisation criteria for the studied multi-area LFC model.

3.1 | Stability analysis with improved Lyapunov function and integral inequalities

Theorem 1. For given constant $\lambda_m, d_1, d_2, \hat{d}$, if there exist positive definite matrices $P_r, Q_{1r}, Q_{2r}, Q_{3r}, R_{1r}, R_{2r}, R_{3r}, \Phi_r$, appropriate dimensions S_1, S_2, S_3, S_4 , and the following LMIs hold for all $r = 0, \dots, L$, the studied LFC model (14) with $\tilde{\omega}(k) = 0$ is asymptotically stable.

$$\tilde{\Phi}_{1r}(d_1) = \Phi_{1r} + H(d_1) < 0, \quad (15)$$

$$\tilde{\Phi}_{1r}(d_2) = \Phi_{1r} + H(d_2) < 0, \quad (16)$$

$$\Theta_{1r} = \sum_{j=1}^L \pi_{rj} (Q_{1j} + Q_{3j}) - R_3 < 0, \quad (17)$$

$$\Theta_{2r} = \sum_{j=1}^L \pi_{rj} (Q_{2j} + Q_{3j}) - R_3 < 0, \quad (18)$$

$$\Theta_{3r} = \sum_{j=1}^L \pi_{rj} Q_{2j} - R_3 < 0, \quad (19)$$

$$\bar{R}_3 = \begin{bmatrix} \bar{R}_1 - \bar{S}_3 & \bar{X}^T \\ \bar{X} & \bar{R}_2 - \bar{S}_4 \end{bmatrix} > 0, \quad (20)$$

where

$$\begin{aligned} \Phi_{1r} &= \Pi_{1r} + \Pi_{2r}, \Pi_{1r} = e_1^T \nu_{1r} e_1 + e_3^T \nu_{3r} e_3 \\ &\quad - H_1^T \hat{R}_1 H_1 - H_2^T \varphi_1 H_2 - H_3^T \varphi_2 H_3 - H_4^T \varphi_3 H_4 \\ &\quad - H_5^T \varphi_4 H_5 - H_8^T \bar{R}_3 H_8 - e_4^T Q_{2r} e_4 - (1 - \hat{d}) e_5^T Q_{2r} \\ &\quad e_5 + \lambda e_5^T \Phi_r e_5 - e_2^T \Phi_r e_2, \Pi_{2r} = \chi_1^T \nu_{2r} \chi_1, \end{aligned}$$

$$H(d_1) = 2H_9^T P_r H_{10} + H_{10}^T \sum_{j=1}^L \pi_{rj} P_j H_{10}$$

$$H(d_2) = 2H_9^T P_r H_{11} + H_{11}^T \sum_{j=1}^L \pi_{rj} P_j H_{11}$$

$$\chi_1 = A e_1 - BK_r C e_2 - BK_r C e_5,$$

$$\nu_{1r} = Q_{1r} + Q_{3r} + d_{12} R_{3r}$$

$$\nu_{2r} = d_1^2 R_{1r} + d_{12}^2 R_{2r} + \frac{d_1^2}{2} S_1 + \frac{d_1^2}{2} S_2 + \frac{d_{12}^2}{2} S_3 + \frac{d_{12}^2}{2} S_4$$

$$\nu_{3r} = Q_{2r} - Q_{1r}, \nu_{4r} = S_1 - d_1 \sum_{j=1}^L \pi_{rj} R_{1j}$$

$$\nu_{5r} = S_3 - d_{12} \sum_{j=1}^L \pi_{rj} R_{2j}, \hat{R}_1 = \text{diag}(R_{1r}, 3R_{1r}, 5R_{1r})$$

$$\varphi_1 = \text{diag}(2\nu_{4r}, 4\nu_{4r}), \varphi_2 = \text{diag}(2\nu_{5r}, 4\nu_{5r}, 2\nu_{5r}, 4\nu_{5r})$$

$$\varphi_3 = \text{diag}(2S_2, 4S_2), \varphi_4 = \text{diag}(2S_4, 4S_4, 2S_4, 4S_4)$$

$$\bar{R}_1 = \text{diag}(R_{2r} + S_3, 3(R_{2r} + S_3), 5(R_{2r} + S_3))$$

$$\bar{R}_2 = \text{diag}(R_{2r} + S_4, 3(R_{2r} + S_4), 5(R_{2r} + S_4))$$

$$\bar{S}_3 = \text{diag}(S_3, 3S_3, 5S_3), \bar{S}_4 = \text{diag}(S_4, 3S_4, 5S_4)$$

$$H_1 = [e_1 - e_3 e_1 + e_3 - 2e_6 e_1 - e_3 + 6e_6 - 6e_9]$$

$$\begin{aligned}
 H_2 &= [e_1 - e_6 \ e_1 + 2e_6 - 3e_9] \\
 H_3 &= [e_3 - e_7 \ e_3 + 2e_7 - 3e_{10}e_5 - e_8 \ e_5 + 2e_8 - 3e_{11}] \\
 H_4 &= [e_6 - e_3 \ e_3 - 4e_6 + 3e_9] \\
 H_5 &= [e_7 - e_5 \ e_5 - 4e_7 + 3e_{10}e_8 - e_4 \ e_4 - 4e_8 + 3e_{11}] \\
 H_6 &= [e_3 - e_5 \ e_3 + e_5 - 2e_7 \ e_3 - e_5 + 6e_7 - 6e_{10}] \\
 H_7 &= [e_5 - e_4 \ e_5 + e_4 - 2e_8 \ e_5 - e_4 + 6e_8 - 6e_{11}] \\
 H_8 &= [H_6 \ H_7]^T, H_9 = [\chi_1 \ e_1 - e_3 \ e_3 - e_4 \ 2(e_1 - e_6)] \\
 H_{10} &= [e_1 \ d_1 e_6 \ d_{12} e_8 \ d_1 e_9], H_{11} = [e_1 \ d_1 e_6 \ d_{12} e_7 \ d_1 e_9], \\
 e_j &= \left[\underbrace{0 \dots 0}_{j-1}, 1, \underbrace{0 \dots 0}_{11-j} \right], (j = 1, \dots, 11).
 \end{aligned}$$

Proof: Construct the Lyapunov function as the following:

$$\begin{aligned}
 V(t) &= \eta^T(t)P\eta(t) + \int_{t-d_1}^t x^T(s)Q_{1r}x(s)ds \\
 &+ \int_{t-d_2}^{t-d_1} x^T(s)Q_{2r}x(s)ds + \int_{t-d(t)}^t x^T(s)Q_{3r}x(s)ds \\
 &+ d_1 \int_{-d_1}^0 \int_{t+\alpha}^t \dot{x}^T(s)R_{1r}\dot{x}(s)dsd\alpha \\
 &+ d_{12} \int_{-d_2}^{-d_1} \int_{t+\alpha}^t \dot{x}^T(s)R_{2r}\dot{x}(s)dsd\alpha \\
 &+ \int_{-d_1}^0 \int_{\beta}^0 \int_{t+\alpha}^t \dot{x}^T(s)S_1\dot{x}(s)dsd\alpha d\beta \\
 &+ \int_{-d_1}^0 \int_{-d_1}^{\beta} \int_{t+\alpha}^t \dot{x}^T(s)S_2\dot{x}(s)dsd\alpha d\beta \\
 &+ \int_{-d_2}^{-d_1} \int_{\beta}^{-d_1} \int_{t+\alpha}^t \dot{x}^T(s)S_3\dot{x}(s)dsd\alpha d\beta \\
 &+ \int_{-d_2}^{-d_1} \int_{-d_2}^{\beta} \int_{t+\alpha}^t \dot{x}^T(s)S_4\dot{x}(s)dsd\alpha d\beta,
 \end{aligned} \tag{21}$$

where

$$\eta(t) = \begin{bmatrix} x(t) \int_{-d_1}^0 x(t+\alpha)d\alpha \int_{-d_2}^{-d_1} x(t+\alpha)d\alpha \\ \frac{2}{d_1} \int_{-d_1}^0 \int_{\beta}^0 x(t+\alpha)d\alpha \end{bmatrix}^T.$$

Calculating the derivative of $V(t)$ along the trajectory of (14) with $\tilde{\omega}(\ell) = 0$ yields

$$\begin{aligned}
 \dot{V}(t) &= \eta^T(t) \sum_{j=1}^L \pi_{rj} P_j \eta(t) + x^T(t) \nu_{1r} x(t) + 2\eta^T(t) P_r \eta(t) \\
 &- (1 - \dot{d}(t)) x^T(t-d(t)) Q_{2r} x(t-d(t)) \\
 &- x^T(t-d_2) Q_{2r} x(t-d_2) + x^T(t-d_1) \nu_{3r} x(t-d_1) \\
 &+ \dot{x}^T(t) \nu_{2r} \dot{x}(t) - d_1 \int_{t-d_1}^t \dot{x}^T(s) \sum_{j=1}^L \pi_{rj} R_{1j} \dot{x}(s) ds \\
 &- \int_{-d_1}^0 \int_{t+\alpha}^t \dot{x}^T(s) \nu_{4r} \dot{x}(s) dsd\alpha \\
 &- \int_{-d(t)}^{-d_1} \int_{t+\alpha}^{t-d_1} \dot{x}^T(s) \nu_{5r} \dot{x}(s) dsd\alpha \\
 &- \int_{-d_2}^{-d(t)} \int_{t+\alpha}^{t-d(t)} \dot{x}^T(s) \nu_{5r} \dot{x}(s) dsd\alpha \\
 &- \int_{-d_1}^0 \int_{t-d_1}^{t+\alpha} \dot{x}^T(s) S_2 \dot{x}(s) dsd\alpha \\
 &- \int_{-d(t)}^{-d_1} \int_{t-d(t)}^{t+\alpha} \dot{x}^T(s) S_4 \dot{x}(s) dsd\alpha \\
 &- \int_{-d_2}^{-d(t)} \int_{t-d_2}^{t+\alpha} \dot{x}^T(s) S_4 \dot{x}(s) dsd\alpha \\
 &+ \int_{t-d_1}^t x^T(s) \Theta_{1l} x(s) ds + \int_{t-d(t)}^{t-d_1} x^T(s) \Theta_{2l} x(s) ds \\
 &+ \int_{t-d_2}^{t-d(t)} x^T(s) \Theta_{3l} x(s) ds + \tilde{V}(t),
 \end{aligned} \tag{22}$$

where

$$\begin{aligned}
 \tilde{V}(t) &= -d_{12} \int_{t-d_{12}}^{t-d_1} \dot{x}^T(s) \sum_{j=1}^L \pi_{rj} R_{2j} \dot{x}(s) ds \\
 &- (d_2 - d(t)) \int_{t-d(t)}^{t-d_1} \dot{x}^T(s) S_3 \dot{x}(s) ds \\
 &- (d(t) - d_1) \int_{t-d_2}^{t-d(t)} \dot{x}^T(s) S_4 \dot{x}(s) ds.
 \end{aligned}$$

Define the augmented vector as follows:

$$\xi(t) = \begin{bmatrix} x(t) \ e(t) \ x(t-d_1) \ x(t-d_2) \end{bmatrix}$$

$$\begin{aligned}
& x(t-d(t)) \frac{1}{d_1} \int_{-d_1}^0 x(t+\alpha) d\alpha \\
& \frac{1}{d(t)-d_1} \int_{-d(t)}^{-d_1} x(t+\alpha) d\alpha \frac{1}{d_2-d(t)} \int_{-d_2}^{-d(t)} x(t+\alpha) d\alpha \\
& \frac{2}{d_1^2} \int_{-d_1}^0 \int_{t+\beta}^t x(\alpha) d\alpha d\beta \frac{2}{(d(t)-d_1)^2} \int_{-d(t)}^{-d_1} \int_{t+\beta}^{t-d_1} x(\alpha) d\alpha d\beta \\
& \left. \frac{2}{(d_2-d(t))^2} \int_{-d_2}^{-d(t)} \int_{t+\beta}^{t-d(t)} x(\alpha) d\alpha d\beta \right]
\end{aligned}$$

By applying Lemma 1, Lemma 2, and reciprocal convex combination approach in [38] with $\alpha = \frac{d(t)-d_1}{d_{12}}$ and $\beta = \frac{d_2-d(t)}{d_{12}}$, if $\bar{R}_3 > 0$ is stabilised, the following inequality can be obtained.

$$\tilde{V}(t) \leq \xi^T(t) \{-H_8^T \bar{R}_3 H_8\} \xi(t). \quad (23)$$

Taking AEt scheme into consideration, it yields

$$\begin{aligned}
\Delta V(t) + \lambda(t_k) x^T(t-d(t)) \Phi_r x(t-d(t)) \\
-e^T(t) \Phi_r e(t) < 0. \quad (24)
\end{aligned}$$

Employing double integral inequalities, (17)–(19), and recalling the augmented vector $\xi(t)$, the next inequality can be satisfied.

$$\xi^T(t) \tilde{\Phi}_{1r} \xi(t) < 0. \quad (25)$$

Thus, the condition (15) and (16) can be derived. With a condition that $\tilde{\omega}(k) = 0$, if (15)–(20) are satisfied, there exists a sufficiently small scalar $\epsilon \in (0, 1]$, such that $\Delta V(k) < -\epsilon \|\xi_1(t)\|^2 < 0$ can be obtained. Therefore, we can confirm that the system (14) with $\tilde{\omega}(k) = 0$ is asymptotically stable.

Remark 2. The improved Lyapunov function is applied in this section. Then, the utilisation of double integral inequalities in $V(t)$ can estimate the upper bounds of transmission time delays. Besides, the integral inequalities with auxiliary functions are applied in $\tilde{V}(t)$ with $\alpha = \frac{d(t)-d_1}{d_{12}}$ and $\beta = \frac{d_2-d(t)}{d_{12}}$. In this way, tighter upper bounds can be given than those obtained by [20, 36]. On the other hand, the double integral term is employed in $\eta(t)$ to analyse the stability of the multi-area LFC model giving less conservative conditions. Moreover, non-quadratic Lyapunov function can add another degree of freedom which can be applied to improve the performance further [39, 40]. This will be investigated in our future work.

Next, the criterion of H_∞ stability about the multi-area LFC model (14) will be designed.

Theorem 2. For given constant $\lambda_m, d_1, d_2, \dot{d}$, if there exists positive definite matrices $P_r, Q_{1r}, Q_{2r}, Q_{3r}, R_{1r}, R_{2r}, R_{3r}, \Phi_r$, appropriate dimensions S_1, S_2, S_3, S_4 , and the following LMIs hold for all $r = 0, \dots, L$, the multi-area LFC model (14) is asymptotically stable with an H_∞ norm bound γ .

$$\tilde{\Phi}'_{1r}(d_1) = \Phi'_{1r} + H'(d_1) - \gamma^2 e_{12}^T e_{12} + e_1^T C^T C e_1 < 0 \quad (26)$$

$$\tilde{\Phi}'_{1r}(d_2) = \Phi'_{1r} + H'(d_2) - \gamma^2 e_{12}^T e_{12} + e_1^T C^T C e_1 < 0 \quad (27)$$

$$\Theta_{1r} < 0, \Theta_{2r} < 0, \Theta_{3r} < 0, \bar{R}_3 > 0$$

where

$$\Phi'_{1r} = \Pi_{1r} + \Pi'_{2r}, \Pi'_{2r} = \chi_1'^T \nu_{2r} \chi_1'$$

$$H'(d_1) = 2H_9'^T P_r H_{10} + H_{10}^T \sum_{j=1}^L \pi_{rj} P_j H_{10}$$

$$H'(d_2) = 2H_9'^T P_r H_{11} + H_{11}^T \sum_{j=1}^L \pi_{rj} P_j H_{11}$$

$$\chi_1' = A e_1 - B K_r C e_2 - B K_r C e_5 + \bar{F} e_{12}$$

$$H_9' = [\chi_1' e_1 - e_3 e_3 - e_4 2(e_1 - e_6)]$$

$$e_j = [\underbrace{0 \dots 0}_{j-1}, 1, \underbrace{0 \dots 0}_{12-j}], (j = 1, \dots, 12)$$

For prescribed attenuation level $\gamma > 0$, considering the disturbance $\tilde{\omega}(t)$, the cost function J is considered:

$$J = \int_0^\infty y^T(t) y(t) - \gamma^2 \tilde{\omega}^T(t) \tilde{\omega}(t) dt \quad (28)$$

Define the augmented vector as

$$\xi'(t) = [\xi(t) \tilde{\omega}(t)]$$

Recalling the condition (25), and applying the same method in Theorem 1, the condition (26) and (27) can be derived. Therefore, the model (14) is asymptotically stable with an H_∞ norm bound γ .

Remark 3. Theorem 1 and Theorem 2 provide sufficient conditions for the stability of the multi-area LFC model. However, the upper bounds of time delays cannot be obtained from the two theorems directly. For the given \dot{d} and the minimum value of the time delay d_1 , the delay margin is increased step by step until the LMIs in Theorem 2 cannot be satisfied. Then, the upper bound of time delay d_2 can be obtained.

3.2 | Stabilisation analysis

In this section, stabilisation criterion of the system (14) will be derived. Then, the fractional-order global sliding mode

controller gain will be designed. Besides, to keep better stabilisation performance, the minimum H_∞ performance index γ are considered.

Theorem 3. For given constant $\lambda_m, d_1, d_2, \dot{d}$, if there exists positive definite matrices $P_r, Q_{1r}, Q_{2r}, Q_{3r}, R_{1r}, R_{2r}, R_{3r}, \Phi_r$, appropriate dimensions S_1, S_2, S_3, S_4 , and the following LMIs hold for all $r = 0, \dots, L$, the power system (14) is asymptotically stable with an H_∞ norm bound γ , and the feedback controller gain can be obtained as \tilde{K}_r .

$$\min \delta$$

$$s.t. \begin{cases} \tilde{\Phi}''_{1r}(d_1) < 0, \tilde{\Phi}''_{1r}(d_2) < 0, \\ \Theta_{1r} < 0, \Theta_{2r} < 0, \Theta_{3r} < 0, \tilde{R}_3 > 0, \end{cases} \quad (29)$$

where

$$\delta = \gamma^2, \tilde{\Phi}''_{1r}(d_1) = \begin{bmatrix} \Phi''_{1r}(d_1) & * \\ \Phi'_{21r} & \Phi'_{22r} \end{bmatrix}$$

$$\tilde{\Phi}''_{1r}(d_2) = \begin{bmatrix} \Phi''_{1r}(d_2) & * \\ \Phi'_{21r} & \Phi'_{22r} \end{bmatrix}$$

$$\Phi''(d_1) = \Pi_{1r} + H'(d_1) - \gamma^2 e_{12}^T e_{12} + e_1^T C^T C e_1$$

$$\Phi''(d_2) = \Pi_{1r} + H'(d_2) - \gamma^2 e_{12}^T e_{12} + e_1^T C^T C e_1$$

$$\chi''_1 = P_r A e_1 - \tilde{K}_r C e_2 - \tilde{K}_r C e_5 - P_r \tilde{F}_{12}$$

$$\Phi'_{21r} = \left[d_1 \chi''_1{}^T \quad d_{12} \chi''_1{}^T \quad \left(d_1 \sqrt{2} \right) \chi''_1{}^T \right.$$

$$\left. \left(d_{12} \sqrt{2} \right) \chi''_1{}^T \quad \left(d_1 \sqrt{2} \right) \chi''_1{}^T \quad \left(d_{12} \sqrt{2} \right) \chi''_1{}^T \right]^T$$

$$\Phi'_{22r} = \text{diag}(R_{1r} - 2P_r, R_{2r}$$

$$- 2P_r, S_1 - 2P_r, S_2 - 2P_r, S_3 - 2P_r, S_4 - 2P_r).$$

Recalling (26), (27) and employing Lemma 1, it yields

$$\begin{bmatrix} \Phi''_{1r}(d(t)) & * \\ \Phi_{21r} & \Phi_{22r} \end{bmatrix} < 0, \quad (30)$$

where

$$\Phi_{21r} = \left[d_1 \chi''_1{}^T \quad d_{12} \chi''_1{}^T \quad \left(d_1 \sqrt{2} \right) \chi''_1{}^T \quad \left(d_{12} \sqrt{2} \right) \chi''_1{}^T \right.$$

$$\left. \left(d_1 \sqrt{2} \right) \chi''_1{}^T \quad \left(d_{12} \sqrt{2} \right) \chi''_1{}^T \right]^T$$

$$\Phi_{22r} = \text{diag}(-R_{1r}^{-1}, -R_{2r}^{-1}, -S_1^{-1}, -S_2^{-1}, -S_3^{-1}, -S_4^{-1}).$$

Pre-multiplying and post-multiplying both sides of (30) with $\text{diag}\{I, \dots, I, P_r, P_r, P_r, P_r, P_r, P_r\}$, and utilising the fact that $Z < 0, Y^T = Y$, then $Y^T Z Y \leq -2Y - Z^{-1}$ can be obtained, and $\tilde{\Phi}''_{1r}(d_1) < 0$ and $\tilde{\Phi}''_{1r}(d_2) < 0$ can be further converted.

TABLE 2 Parameters of the two-area LFC scheme

Area	R	M	D	T_g	T_{ch}	T_{12}
1	0.05	10.0	1.0	0.1	0.3	0.1986
2	0.05	12.0	1.5	0.17	0.4	0.1986

Therefore, the theorem is proved and the controller gain is $\tilde{K}_r = P_r K_r$.

Remark 4. In this theorem, the H_∞ stabilisation for the multi-area power system LFC is investigated. Then, the controller of the multi-area power system LFC can be designed in this remark under the minimum γ condition. By utilising the mincx function in the Matlab LMI toolbox, the less conservative results of the controller gain is obtained.

Theorem 4. A decentralised switching control law can be designed as following to guarantee the reaching condition $s(t)\dot{s}(t) < 0$.

$$u(t) = -K_r C x(t) + (GB)^{-1} \dot{f}(t) - \mu (GB)^{-1} D^{\alpha_1} x(t)$$

$$+ k(\text{sgn}(s(t)) + s(t)) \quad (31)$$

The proof of this theorem is the same as [36]. In this theorem, the fractional-order global sliding mode controller is designed. It forces the state trajectories to move towards the sliding surface within a finite time. Therefore, it can greatly improve the system transient performance.

4 | CASE STUDY AND DISCUSSION

The effectiveness and superiority of the proposed AEt and FOGSMC scheme are discussed in this section. In Case 1, the two-area power system model is built with Matlab/Simulink, and the LMI toolbox in Matlab is applied to compute the stability margin of transmission time delays with different controller gains. The parameters are tabulated as shown in Table 2. Additionally, in Case 2, IEEE 39-bus system is implemented to validate the performance of the proposed FOGSMC scheme in a realistic power system condition.

4.1 | Case 1: Two-area power system LFC

In this case, two-area LFC model with two wind farms and two energy storage units are built as shown in Figure 2. The detail parameters are in [36]. As shown in Figure 3(a), the transition probability matrix will be selected as following:

$$P = \begin{bmatrix} 0.5088 & 0.4912 \\ 0.4286 & 0.5714 \end{bmatrix}.$$

By solving Theorem 2, the stability margin of transmission time delays for different controller gains can be derived. Table 3

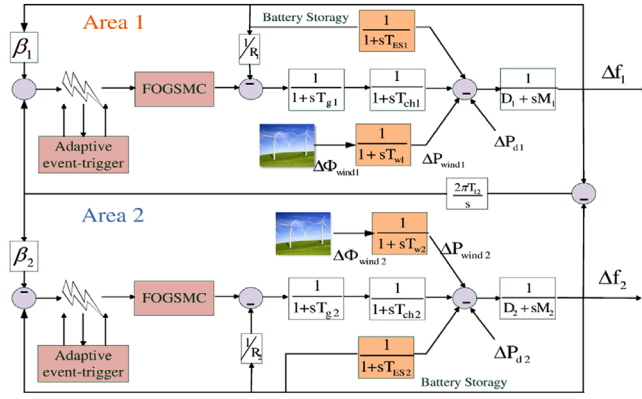


FIGURE 2 Transfer function model of two-area power system with wind farm and energy storage unit

TABLE 3 Transmission time delay upper bound comparison

K_I	K_p	$d = 0.0$			$d = 0.5$		
		This paper	[41]	[42]	This paper	[41]	[42]
0.0	0.1	14.55	13.77	13.77	14.01	11.72	12.88
0.0	0.2	7.46	6.69	6.69	6.94	5.55	6.14
0.0	0.4	2.72	3.12	3.12	2.44	2.36	2.68
0.1	0.2	7.80	6.88	6.94	3.48	5.83	6.34
0.1	0.4	3.98	3.29	3.17	3.24	2.55	2.83
0.1	0.6	2.72	1.86	3.12	2.44	1.31	1.57

compares the obtained results with those in [41] and [42] under $\hat{d} = 0.0, \hat{d} = 0.5$ condition. It can be concluded that the upper bounds of the transmission time delays obtained by the proposed method are larger than those in [41] and [42]. Therefore, the proposed method — improved Lyapunov function and the integral inequalities with auxiliary functions — has a better performance in calculating the upper bounds of time delays under stable condition.

In light of Theorem 3 with $\lambda_m = 0.1, \gamma = 2.8422$ can be obtained and fractional order global sliding mode controller can be designed as the following:

$$u(t) = -K_{ij}Cx(t) + 4.0\dot{f}(t) - 0.001(s(t) + \text{sgn}(s(t))) - 0.08D^{0.92}x(t)$$

where Area 1: $K_{11} = [0.0986, 0.0097], K_{12} = [0.0989, 0.0097]$

Area 2: $K_{21} = [0.0810, 0.0119], K_{22} = [0.0815, 0.0121]$

In the built two-area power system, the wind turbine induction generator with 9 m/s wind speed and 0.2 trip coefficient is applied. The power deviations of wind turbine governor and generators are curved in Figure 3(c) and (d). For AEt scheme with $\lambda_m = 0.1$, the release time instants and intervals are depicted in Figure 3(b). It can be observed that the proposed AEt scheme can reduce the unnecessary information exchange and relieve transmission burden.

Figure 4(a) describes the sliding surfaces which converge to zero in a short time. It demonstrates that the designed system reaches the sliding surfaces asymptotically and remains on the sliding surfaces. The proposed FOGSMC scheme is compared with three representative AEt-based scheme, that is, SMC [20], PI control, and fractional order PID (FOPID) control [2] under step load disturbances, as shown in Figure 4(b)–(d). It can be observed that the proposed FOGSMC scheme exhibits lower overshoot, faster response and greater damping in the frequency deviations and ACEs than other mentioned methods. Detailed parameters of other controllers are listed in the Appendix.

Parameter uncertainty is a major issue for power systems. To investigate robustness of the proposed method, frequency deviations of FOGSMC and other three methods under $\pm 50\%$ parameter uncertainty are compared in Figure 5. It can be observed that the designed FOGSMC scheme manifests distinguished robustness compared to the existing SMC, PI control, and FOPID control scheme.

To scrutinise the utility of the proposed FOGSMC with the presence of non-linearities, the governor dead band (GDB) and generation rate constraint (GRC) are considered in the two-area LFC study case. With the GDB width $D = 0.05\%$ and 0.1 p.u./min GRC, the frequency deviation and ACE are illustrated in Figure 6(a) and (b), respectively. It can be observed that the frequency deviation and ACE response can converge to zero in a short time and exhibit good disturbance rejection capability.

4.2 | Case 2: Modified IEEE 39-bus New England test system

To validate the effectiveness of the designed FOGSMC scheme in a more realistic power system model, a modified IEEE 39-bus power system with three wind farms is built as shown in Figure 7. The detail parameters can be obtained in [43]. There are 10 generators, 19 loads, 34 transmission lines, and 12 transformers in the IEEE 39-bus test system, and three wind farms with the capacities of 380 MW, 445 MW, and 500 MW are integrated to bus 1, 9, and 19, respectively. This test system is split into three control areas, shown as Figure 7, where G_3 in Area 1, G_7 in Area 2, and G_9 in Area 3 are responsible for the LFC performance in each control area, respectively. The FOGSMC scheme is elucidated as the following:

$$u(t) = -0.9x(t) + 0.7 \int_0^t x(s)ds + 0.1\dot{f}(t) + 21s(t) - 0.01\text{sgn}(s(t)) - 14D^{0.92}x(t),$$

where

$$s(t) = x(t) + 4 \int_0^t x(s)ds + 0.1653f(t) + 14D^{-0.08}x(t).$$

In this case, the step load disturbances 0.038 p.u. MW on Bus 8 at $t = 30$ s in Area 1, 0.064 p.u. MW on Bus 16 at $t = 60$ s in Area 2, and 0.038 p.u. MW on Bus 3 at $t = 90$ s in Area 3 are considered. It can be observed in Figure 8(a) and (b) that the proposed FOGSMC scheme can maintain stability of this system, and the frequency deviation and tie-line power deviation of three control areas can converge to zero in a short time with inconspicuous overshoots and satisfactory transient performance.

FIGURE 3 Results of two-area LFC: (a) Random transmission delays, (b) Release instant and release intervals for Area 1, (c) Wind turbine governor output power deviation, (d) Generator output power deviation for Area 1 and Area 2

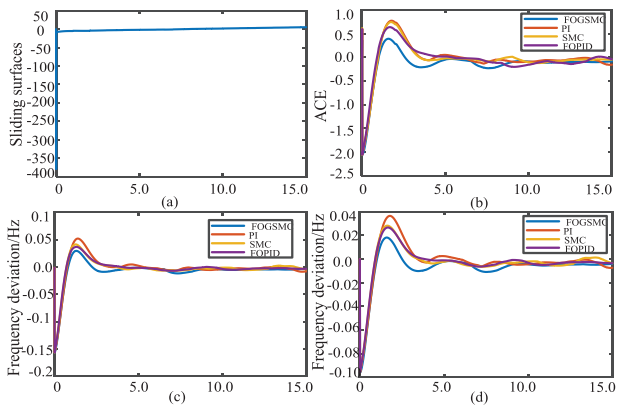
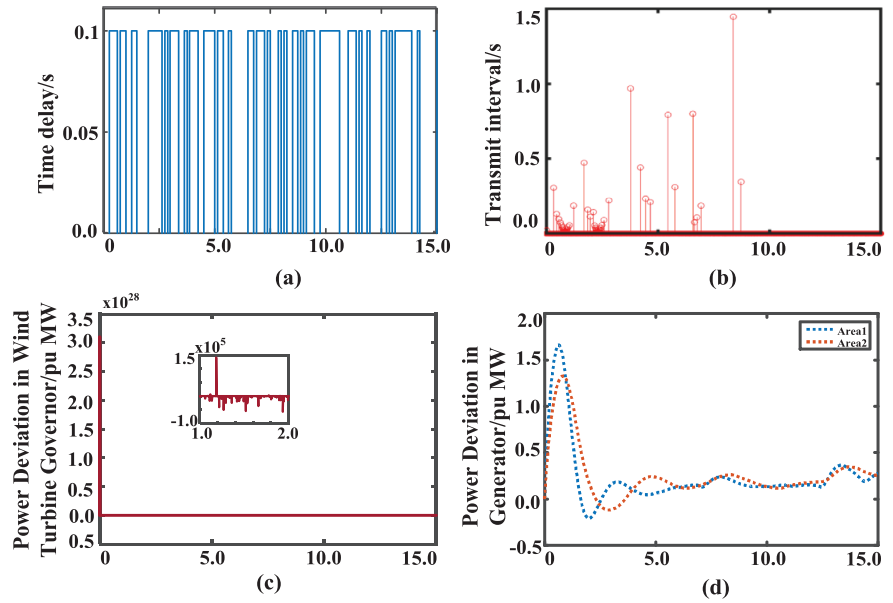


FIGURE 4 Results with step load disturbances: (a) Sliding surfaces, (b) ACE for Area 2, (c) Frequency deviations for Area 1, (d) Frequency deviations for Area 2

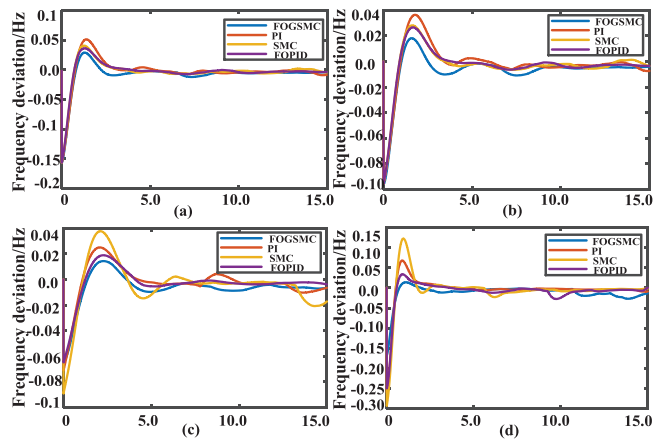


FIGURE 5 Frequency deviations with uncertainty parameter: (a) +50% uncertainty parameter in Area 1, (b) +50% uncertainty parameter in Area 2, (c) -50% uncertainty parameter in Area 1, (d) -50% uncertainty parameter in Area 2

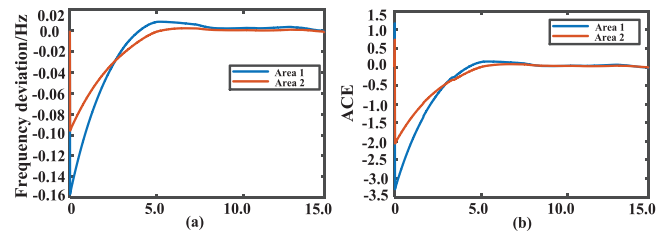


FIGURE 6 Frequency deviations and ACE for GRC and GDB condition

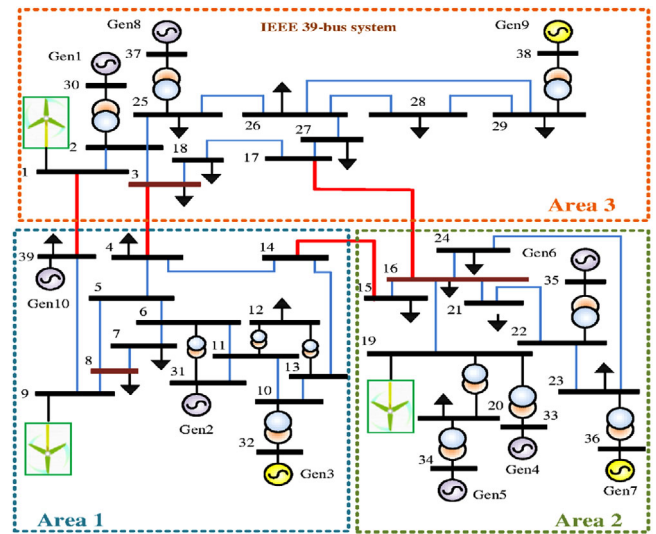


FIGURE 7 Modified IEEE 39 bus test system

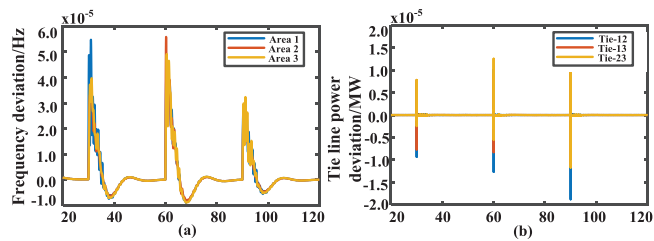


FIGURE 8 Frequency deviations and tie line power deviations of modified IEEE 39-bus test system

5 | CONCLUSION

The stability and stabilisation of the LFC scheme for power systems with renewable energy have been studied in this paper. The Markov jump linear theory is applied to describe the delay dependent multi-area LFC model. By utilising the improved Lyapunov function and integral inequalities, the stability and stabilisation criteria with less conservativeness are derived. The AEt scheme with an adjustable triggering threshold can effectively economise the network resources. The proposed FOGSMC scheme exploiting advantages of fractional term and GSMC is first applied in this LFC system. Compared with existing AEt-based control schemes, the FOGSMC based on AEt scheme exhibits outstanding disturbance rejection performance and demonstrates better robustness under $\pm 50\%$ parameter uncertainty. In addition, it presents satisfactory performance under non-linearity of GDB and GRC conditions. Finally, the effectiveness of the proposed FOGSMC scheme in the realistic power system is verified by the IEEE 39-bus test system with three wind farms.

ACKNOWLEDGMENTS

This work was supported in part by the National Natural Science Foundation of China under Grant 62073121, and in part by the Natural Science and Engineering Research Council (NSERC) of Canada, in part by Six Talent Peaks High Level Project of Jiangsu Province under Grant 2017-XNY004, and in part by the Innovation Team of Six Talent Peaks Project of Jiangsu Province under grant 2019-TD-XNY-001. X. Lv was supported by the China Scholarship Council.

ORCID

Xinxin Lv  <https://orcid.org/0000-0001-5007-2123>

Wenqiang Hu  <https://orcid.org/0000-0003-2632-8170>

Venkata Dinavahi  <https://orcid.org/0000-0001-7438-9547>

REFERENCES

- Liu, S., Liu, P.: Distributed model-based control and scheduling for load frequency regulation of smart grids over limited bandwidth networks. *IEEE Trans. Ind. Inf.* 14(5), 1814–1823 (2018)
- Abazari, A., et al.: Load frequency control by de-loaded wind farm using the optimal fuzzy-based PID droop controller. *IET Renew. Power Gener.* 13(1), 180–190 (2018)
- Golkhandan, R. et al.: Load frequency control of smart isolated power grids with high wind farm penetrations. *IET Renew. Power Gener.* 14(7), 1228–1238 (2020)
- Hou, Q. et al.: Impact of high renewable penetration on the power system operation mode: A data-driven approach. *IEEE Trans. Power Syst.* 35(1), 731–741 (2020)
- Patel, R. et al.: Enhancing optimal automatic generation control in a multi-area power system with diverse energy resources. *IEEE Trans. Power Syst.* 34(5), 3465–3475 (2019)
- Martinez, M., et al.: Optimal sizing method of vanadium redox flow battery to provide load frequency control in power systems with intermittent renewable generation. *IET Renew. Power Gener.* 11(14), 1804–1811 (2017)
- Li, H., et al.: Adaptive event-triggered load frequency control for interconnected microgrids by observer-based sliding mode control. *IEEE Access* 768271–68280 (2019)
- Onyeka, A. et al.: Robust decentralised load frequency control for interconnected time delay power systems using sliding mode techniques. *IET Control Theory Appl.* 14(3), 470–480 (2020)
- Jia, Y. et al.: Cooperation-based distributed economic MPC for economic load dispatch and load frequency control of interconnected power systems. *IEEE Trans. Power Syst.* 34(5), 3964–3966 (2019)
- Vafamand, N. et al.: Time-delayed stabilizing secondary load frequency control of shipboard microgrids. *IBM Syst. J.* 13(3), 3233–3241 (2019)
- Peng, C., et al.: Adaptive event-triggering H_∞ load frequency control for network-based power systems. *IEEE Trans. Ind. Electron.* 65(2), 1685–1694 (2018)
- Zhang, H., et al.: H-infinity load frequency control of networked power systems via an event-triggered scheme. *IEEE Trans. Ind. Electron.* 67(8), 7104–7113 (2020)
- Wen, S. et al.: Event-triggering load frequency control for multiarea power systems with communication delays. *IEEE Trans. Ind. Electron.* 63(2), 1308–1317 (2016)
- Dong, L. et al.: An event-triggered approach for load frequency control with supplementary ADP. *IEEE Trans. Power Syst.* 32(1), 581–589 (2017)
- Liu, J. et al.: Event-triggered H_∞ load frequency control for multiarea power systems under hybrid cyber attacks. *IEEE Trans. Syst. Man Cybern. Syst.* 49(8), 1665–1678 (2019)
- Yuan, Y. et al.: Noncooperative event-triggered control strategy design with round-robin protocol: Applications to load frequency control of circuit systems. *IEEE Trans. Ind. Electron.* 67(3), 2155–2166 (2020)
- Chuang, N.: Robust H_∞ load-frequency control in interconnected power systems. *IET Control Theory Appl.* 10(1), 67–75 (2016)
- Jain, S., Hote, Y.: Generalized active disturbance rejection controller for load frequency control in power systems. *IEEE Control Syst. Lett.* 4(1), 73–78 (2020)
- Ramadan, H., et al.: Optimal gain scheduling of VSC-HVDC system sliding mode control via artificial bee colony and mine blast algorithms. *IET Gener. Transm. Distrib.* 12(3), 661–669 (2017)
- Sun, Y. et al.: Robust H_∞ load frequency control of multi-area power system with time delay: A sliding mode control approach. *IEEE/CAA J. Autom. Sin.* 5(2), 610–617 (2018)
- Liao, K., Xu, Y.: A robust load frequency control scheme for power systems based on second-order sliding mode and extended disturbance observer. *IEEE Trans. Ind. Inf.* 14(7), 3076–3086 (2018)
- Guo, J.: Application of full order sliding mode control based on different areas power system with load frequency control. *ACA Trans.* 92, 23–34 (2019)
- Mu, C., et al.: Improved sliding mode design for load frequency control of power system integrated an adaptive learning strategy. *IEEE Trans. Ind. Electron.* 64(8), 6742–6751 (2017)
- Trip, S., et al.: Passivity-based design of sliding modes for optimal load frequency control. *IEEE Trans. Control Syst. Technol.* 27(5), 1893–1906 (2019)
- Ma, Z., Ma, H.: Adaptive fuzzy backstepping dynamic surface control of strict-feedback fractional-order uncertain nonlinear systems. *IEEE Trans. Fuzzy Syst.* 28(1), 122–133 (2020)
- Fedele, G.: A fractional-order repetitive controller for periodic disturbance rejection. *IEEE Trans. Autom. Control* 63(5), 1426–1433 (2018)

27. Komathi, C., Umamaheswari, M.: Design of gray wolf optimizer algorithm-based fractional-order PI controller for power factor correction in SMPS applications. *IEEE Trans. Power Electron.* 35(5), 5543–5543 (2020)
28. Tasnin, W., Saikia, L.: Impact of renewables and fact device on deregulated thermal system having sine cosine algorithm optimised fractional order cascade controller. *IET Renew. Power Gener.* 13(9), 1420–1430 (2019)
29. Fei, J., Lu, C.: Adaptive fractional order sliding mode controller with neural estimator. *J. Franklin Inst.* 355(5), 2369–2391 (2018)
30. Xiang, Y., et al.: Robust energy management of microgrid with uncertain renewable generation and load. *IEEE Trans. Smart Grid* 7(2), 1034–1043 (2016)
31. Hosseinzadeh, M., Salmasi, F.: Robust optimal power management system for a hybrid ac/dc micro-grid. *IEEE Trans. Sustain. Energ.* 6(3), 675–687 (2015)
32. Pham, T. et al.: Integration of electric vehicles for load frequency output feedback H ∞ control of smart grids. *IET Gener. Transm. Distrib.* 10(13), 3341–3352 (2016)
33. Jin, L. et al.: Delay-dependent stability analysis of multi-area load frequency control with enhanced accuracy and computation efficiency. *IEEE Trans. Power Syst.* 34(5), 3687–3696 (2019)
34. Li, W. et al.: Adaptive-event-trigger-based fuzzy nonlinear lateral dynamic control for autonomous electric vehicles under insecure communication networks. *IEEE Trans. Ind. Electron.* 68(3), 2447–2459 (2021)
35. Shi, Y., Yu, B.: Output feedback stabilization of networked control systems with random delays modeled by Markov chains. *IEEE Trans. Automat. Contr.* 54(7), 1668–1674 (2009)
36. Lv, X., et al.: Adaptive event-triggered load frequency control of multi-area power systems under networked environment via sliding mode control. *IEEE Access* 8(1), 86585–86594 (2020)
37. Park, P., et al.: Auxiliary function-based integral inequalities for quadratic functions and their applications to time-delay systems. *J. Franklin Inst.* 352(4), 1378–1396 (2015)
38. Yang, F., Zhang, H.: T-s model-based relaxed reliable stabilization of networked control systems with time-varying delays under variable sampling. *Int. J. Fuzzy Syst.* 13(4), 260–269 (2011)
39. Hosseinzadeh, M., Yazdanpanah, M.: Performance enhanced model reference adaptive control through switching non-quadratic Lyapunov functions. *Syst. Control Lett.* 76, 47–55 (2015)
40. Balleateros, M. et al.: Adaptive output control of a mobile manipulator hanging from a quadcopter unmanned vehicle. *ISA Trans.* 94, 200–217 (2019)
41. Jiang, L. et al.: Delay-dependent stability for load frequency control with constant and time-varying delays. *IEEE Trans. Power Syst.* 27(2), 932–941 (2012)
42. Ramakrishnan, K., Ray, G.: Stability criteria for nonlinearly perturbed load frequency systems with time-delay. *IEEE J. Emerging Sel. Top. Circuits Syst.* 5(3), 383–392 (2015)
43. Pai, M.: *Energy Function Analysis for Power System Stability*. Kluwer, Boston, MA (1989)

How to cite this article: Lv X, Sun Y, Hu W, Dinavahi V. Robust load frequency control for networked power system with renewable energy via fractional-order global sliding mode control. *IET Renew Power Gener.* 2021;15:1046–1057.
<https://doi.org/10.1049/rpg2.12088>

APPENDIX A

In Section 4, the SMC has the same controller gain as FOGSMC, except that there is no fractional-order term $D^{0.98}x(t)$ and $f(t)$. The FOPID controller can be designed as

$$u(s) = K_p + K_I \frac{1}{s^t} + K_D s^v.$$

Area 1:

$$K_{11}(K_p, K_I, K_D, t, v) = [0.0986, 0.0097, -0.1, 0.92, 0.92],$$

$$K_{12}(K_p, K_I, K_D, t, v) = [0.0989, 0.0097, -0.1, 0.92, 0.92].$$

Area 2:

$$K_{21}(K_p, K_I, K_D, t, v) = [0.0810, 0.0119, -0.1, 0.92, 0.92],$$

$$K_{22}(K_p, K_I, K_D, t, v) = [0.0815, 0.0121, -0.1, 0.92, 0.92].$$

The PI controller gains are

$$\text{Area 1: } K_{11} = [0.0986, 0.0097], K_{12} = [0.0989, 0.0097],$$

$$\text{Area 2: } K_{21} = [0.0810, 0.0119], K_{22} = [0.0815, 0.0121].$$